Volume 335, number 1, 18–26 FEBS 13281 November 1993

NMR determination of the secondary structure and the three-dimensional polypeptide backbone fold of the human sterol carrier protein 2

T. Szyperski[a,*], S. Scheek[b,c,**], J. Johansson[a], G. Assmann[b,d], U. Seedorf[b], K. Wüthrich[a]

[a]*Institut für Molekularbiologie und Biophysik, Eidgenössische Technische Hochschule-Hönggerberg, CH-8093 Zürich, Switzerland*
[b]*Institut für Arteriosklerosеforschung, Westfälische Wilhelms-Universität, D-4400 Münster, Germany*
[c]*Institut für Biochemie, Westfälische Wilhelms-Universität, D-4400 Münster, Germany*
[d]*Institut für Klinische Chemie und Laboratoriumsmedizin, Zentrallaboratorium, Westfälische Wilhelms-Universität, D-4400 Münster, Germany*

Received 4 October 1993

Nuclear magnetic resonance (NMR) spectroscopy was used to determine the secondary structure and the three-dimensional polypeptide backbone fold of the human sterol carrier protein 2 (hSCP2), which is a basic protein with 123 residues believed to participate in the intracellular transport of cholesterol and various other lipids. Sequence-specific assignments were obtained for nearly all backbone ^{1}H and ^{15}N resonances, as well as for about two-thirds of the side-chain ^{1}H resonances, using uniform ^{15}N-labeling of the protein combined with homonuclear two-dimensional ^{1}H NMR and three-dimensional ^{15}N-correlated ^{1}H NMR. Three α-helices comprising the polypeptide segments of residues 9–22, 25–30 and 78–84 were identified by sequential and medium-range nuclear Overhauser effects (NOE). The analysis of long-range backbone–backbone NOEs showed that hSCP2 further contains a five-stranded β-sheet including the residues 33–41, 47–54, 60–62, 71–76 and 100–102, which is a central feature of the molecular architecture. The first three strands are arranged in an antiparallel fashion, the polypeptide chain then crosses over this three-stranded sheet in a right-handed sense so that the fourth strand is added parallel to the first one. The fifth strand runs antiparallel to the fourth one, so that the overall topology is +1, +1, −3x, −1. The three-dimensional arrangement of the β-sheet and the first two helices was determined using an input of 625 NOE upper distance constraints and 95 scalar coupling constants for a preliminary structure calculation with the distance geometry program DIANA.

Human sterol carrier protein 2; Protein structure; Secondary structure; Nuclear magnetic resonance

1. INTRODUCTION

The sterol carrier protein 2 (SCP2, or 'non-specific lipid transfer protein', NSLTP) is a small basic lipid transfer protein which was originally isolated from rat liver but has since been detected in a number of other tissues and species (see [1,2] for recent reviews). The hypothesis that SCP2 participates in the intracellular transport of sterols and lipids is based upon the finding that the protein catalyses the in vitro transport through membranes of a wide variety of sterols [3] and common lipids [4]. Furthermore, it activates the enzymatic conversion of 7-dehydrocholesterol to cholesterol [5], the acetyl-CoA cholesterol acyltransferase-mediated esterification of cholesterol [6–8], and catalyzes in vitro the introduction of the less polar substrates in bile acid biosynthesis to the membrane-bound enzymes [9,10], suggesting that SCP2 plays an important role in steroid metabolism. Apart from the liver, the protein is most prominently expressed in the adrenals [11], which led to the proposal that SCP2 is likewise required for the intracellular transfer of cholesterol during pregnenolone synthesis in this tissue [11–13]. Furthermore, the recent identification of an oleic acid-inducible SCP2 homologue in *Candida tropicalis* [14] points to a high degree of evolutionary conservation, which is another indication that SCP2 might be of key importance for the cellular lipid metabolism.

In contrast to the wide array of implicated functional roles for SCP2, very little is known so far about the structural basis of these functions. Nucleotide sequencing of SCP2-encoding cDNAs revealed that rat, mouse and human SCP2 are synthesized as 143-amino acid precursor proteins (pre-SCP2), with post-translational processing to the mature SCP2s comprising 123 amino acid residues [15–20]. Purified SCP2 does not contain any bound lipid [11,21], and no high-affinity binding of radio-labeled sterols to SCP2 was observed in vitro [4]. It has therefore been proposed that SCP2 does not function as a typical lipid carrier protein, but might be bound as a connecting tunnel between lipid interphases by electrostatic interactions to membrane surfaces, and thus facilitates transfer of hydrophobic molecules from a donor to an acceptor membrane [4]. Other observations by site-directed mutagenesis of SCP2, however,

*Corresponding author.

**Part of this work was presented in a thesis in partial fulfilment of the requirements of the Westphalian Wilhelms-University, Münster.

favour the existence of a local lipid-binding site [22] and indicate that SCP2 shields the bound lipids from the aqueous phase as would be expected for a typical lipid-carrier protein [23]. To obtain a more detailed structural basis of SCP2-mediated lipid transport, we have started an NMR structure determination in solution. This paper reports sequence-specific resonance assignments and a determination of the secondary structure and the global polypeptide backbone fold.

2. MATERIALS AND METHODS

2.1. *Preparation of human SCP2 with natural isotope content and uniform ^{15}N-labeling*

A cDNA encoding human pre-SCP2 was isolated from a liver λ-gt11 cDNA library (clone pBS-hSCP2; [22]). This clone was used as a template for PCR amplifications using 5′ and 3′ oligonucleotide primers that introduce *Bam*HI and *Eco*RI restriction sites at the 5′ and 3′ ends of the amplified DNA fragments. The DNA fragments thus obtained were digested with *Bam*HI and *Eco*RI, cloned directionally into the corresponding restriction sites of the vector pGEX-2T [24,25], and the resulting construct pGEX-2T/hSCP2 was verified by nucleotide sequencing. *E. coli* XL-1 Blue (Stratagene, La Jolla, USA) transformed with the vector pGEX-2T/hSCP2 were grown to an OD_{600} of ~0.8 in a 20 l bioreactor (MBR - Sulzer, Wetzikon, Switzerland) and expression was induced by the addition of IPTG (Boehringer Mannheim, Mannheim, Germany) to a final concentration of 0.1 mM. After 5 h of further fermentation, the glutathione *S*-transferase (GST) fusion protein was extracted and purified [24,25], dialysed against 100 vol. of phosphate-buffered saline, cleaved by incubation for 2 h at 37°C with 1:20 (w/w) thrombin (Sigma, St. Louis, USA), and GST was then removed by affinity chromatography over glutathione sepharose 4B (Pharmacia, Uppsala, Sweden). The flow-through was dialysed against 100 vol. of 50 mM NaCl, 50 mM Tris-HCl, pH 8.6, and the hSCP2 was further purified to homogeneity via passage over DEAE-Sephadex equilibrated with the same buffer. Protein concentrations were determined using the Bradford assay [26], and sterol carrier and lipid transfer assays of purified recombinant hSCP2 performed as described in [22]. Protein sequencing of the N-terminal 20 residues showed that the recombinant hSCP2 contained an extra N-terminal Gly-Ser dipeptide due to the introduction of the *Bam*HI-linker sequence.

To prepare uniformly ^{15}N-labeled hSCP2, 200 ml of an overnight culture of XL-1 Blue/pGEX-2T/hSCP2 grown in doubly-concentrated yeast tryptone medium were used to inoculate 8 l of a minimal medium consisting of M9 medium supplemented with 60 ml of 20% glucose, 0.5 ml of 2% thiamine, 5 ml of 10 mg/ml of ampicillin, and 1 g of $(NH_4)_2SO_4$ per litre. After growing the bacteria at 37°C on a rotary shaker at 250 rpm to an OD_{600} of 0.6, the culture was collected by centrifugation at 3,000 × *g* for 15 min and resuspended at an OD_{600} of 1.0 in the above minimal medium containing 1 g/l of $(^{15}NH_4)_2SO_4$ and 0.2 mM IPTG. After incubation at 37°C on a rotary shaker at 250 rpm for 8 h, the bacteria were collected by centrifugation at 3,000 × *g* for 15 min and the ^{15}N-labeled hSCP2 was isolated and purified as described above.

For the NMR experiments, 0.3 mM solutions of hSCP2 in 15 mM KH_2PO_4/5 mM dithiothreitol (DTT) at pH = 6.0 were concentrated to about 1.5 mM by ultrafiltration in a Centricon 3 microconcentrator (Amicon, USA) at 22°C. 30 μl of D_2O were added to 400 μl of the concentrated solution, and the sample was kept in a 5 mm NMR tube under argon. NMR spectra were recorded at pH = 6.0. Between NMR measurements the samples were stored at 4°C.

2.2. *NMR spectroscopy*

All NMR spectra were recorded on an Bruker AMX 600 spectrometer and quadrature detection in the indirectly detected dimensions was obtained using the States-TPPI method [27]. For the data processing we used the program PROSA [28]. The ^1H chemical shifts at 36°C are relative to the water resonance at 4.65 ppm from [2,2,3,3-D_4]-trimethylsilyl-propionate (TSP). Two-dimensional (2D) [^1H,^1H]-NOESY spectra with 100 ms mixing time [29] were recorded at 36°C in H_2O and D_2O as data matrices with 256 (t_1) * 512 (t_2) complex points (t_{1max} = 29.2 ms, t_{2max} = 65.5 ms) in approximately 24 h. A clean-TOCSY spectrum [30] in H_2O with a mixing time of 50 ms was recorded with the same data size and measurement time. The intensity of the H_2O signal was suppressed by irradiation during the relaxation delay and further reduced with the convolution method of Marion et al. [31]. The data sets were multiplied in both dimensions with phase-shifted sine-bell functions [32] and the baseline was corrected as described by Güntert and Wüthrich [33]. The digital resolution after zero-filling was 15 Hz along ω_1 and 7.6 Hz along ω_2.

2D and three-dimensional (3D) heteronuclear NMR experiments were performed at 36, 28 and 22°C. The intensity of the H_2O signal was reduced using spin-lock purge pulses [34], and a WALTZ-16 scheme [35] was applied to decouple ^{15}N during the acquisition. **(i)** At 36°C, a 2D [^{15}N,^1H]-HSQC experiment [36] was recorded with 186 (t_1) * 1024 (t_2) complex points (t_{1max} = 100 ms, t_{2max} = 131 ms) and a measurement time of about 24 h. A 3D ^{15}N-resolved [^1H,^1H]-TOCSY experiment [37,38] using a mixing time of 50 ms, a 3D ^{15}N-resolved [^1H,^1H]-NOESY experiment [37–39] using a mixing time of 100 ms, and a 3D *ct*-HNNHB experiment [40,41] were recorded with 32 (t_1) * 212 (t_2) * 512 (t_3) complex points (t_{1max} = 17.3 ms, t_{2max} = 28.0 ms, t_{3max} = 65.5 ms) in about 3 days each. Prior to Fourier transformation the water signal was further reduced by convolution [31], the number of complex points in t_1 was increased to 48 by linear prediction [42], the data sets were multiplied in all dimensions with phase-shifted sine-bell functions [32] and baseline corrected [33]. The digital resolution after zero-filling was 3.6 Hz along ω_1 and 1.9 Hz along ω_2 for the 2D spectrum, and 14.8 Hz, 28.9 Hz, and 7.6 Hz along ω_1, ω_2 and ω_3, respectively, for the 3D spectra. A 2D $^{15}N(\omega_1,\omega_2)$-double-half filter [$^1H$,$^1H$]-NOESY spectrum [43] using a mixing time of 100 ms with 256 (t_1) * 512 (t_2) complex points (t_{1max} = 33.3 ms, t_{2max} = 65.5 ms) was recorded in about 2 days and processed as described above for the [^1H,^1H]-NOESY. **(ii)** At 28°C, 2D [^{15}N,^1H]-HSQC, 3D ^{15}N-resolved [^1H,^1H]-TOCSY and ^{15}N-resolved [^1H,^1H]-NOESY spectra were recorded with similar parameters as in **(i)**. **(iii)** At 22°C, a 2D [^{15}N,^1H]-HSQC, a 2D ^1H-TOCSY- relayed [^{15}N,^1H]-COSY, and a 2D ^1H-NOESY-relayed [^{15}N,^1H]-COSY experiment with a mixing time of 100 ms were recorded with 112 (t_1) * 512 (t_2) complex points (t_{1max} = 60.5 ms, t_{2max} = 131 ms) and processed as described for the 2D [^{15}N,^1H]-HSQC experiment at 36°C. The water chemical shift references used were 4.72 ppm at 28°C, and 4.80 ppm at 22°C.

The vicinal scalar coupling constants $^3J_{NH\alpha}$ were extracted by inverse Fourier transformation of in-phase multiplets from the 2D [^{15}N,^1H]-HSQC spectra at 36°C and 28°C [44].

Slowly exchanging amide protons were identified at 22°C in 2D [^{15}N,^1H]-HSQC experiments of the ^{15}N-labeled protein dissolved in D_2O. The sample was prepared at 4°C over a time period of 5 h, which included dialysis against D_2O and concentration over a Centricon 3 microconcentrator. A series of 2D [^{15}N,^1H]-COSY experiments was acquired, i.e., three groups of 4 spectra with recording times of 15, 30 and 60 min per spectrum, respectively, and 12 spectra with recording times of 4 h each. Data matrices of 96 (t_1) * 1024 (t_2) complex points (t_{1max} = 52 ms, t_{2max} = 65.5 ms) were recorded and processed as described for the other ^{15}N-correlated 2D spectra. The cross peak volumes were integrated using the program EASY [45], and the exchange rates were obtained from a least-squares fit of a single exponential function to the experimental data.

To collect the input for the preliminary structure calculations, the 3D ^{15}N-resolved [^1H,^1H]-NOESY spectra were integrated with the home-written program PEAKINT (N. Schäfer, C. Bartels and K. Wüthrich, unpublished), and NOEs with the aromatic spin systems were integrated in the 2D ^1H-NOESY spectra with the program EASY [45]. The 3D and 2D cross peak volumes were converted to upper distance limits with the program CALIBA [46]. Dihedral angle con-

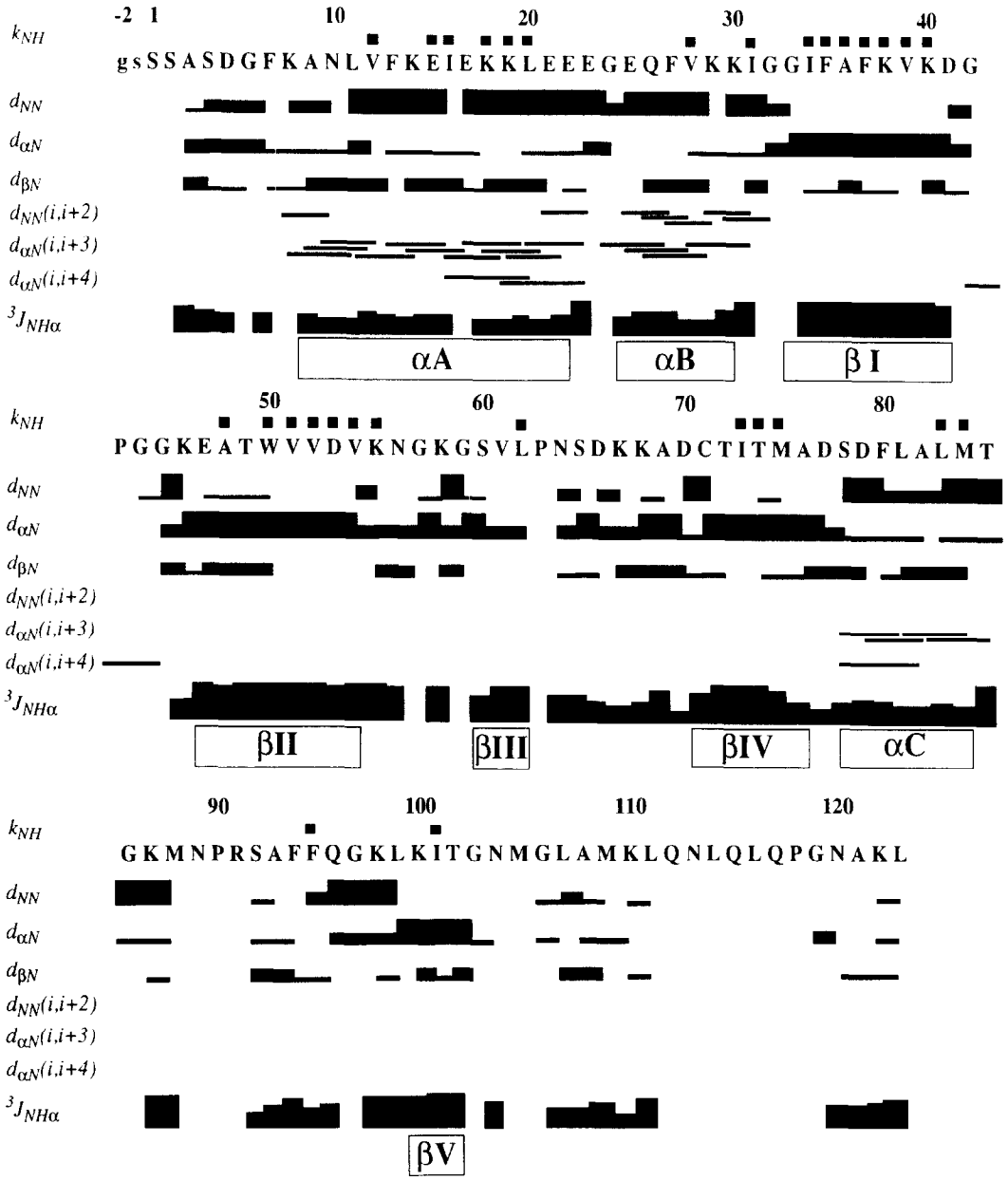

Fig. 1. Amino acid sequence of hSCP2, sequential and medium-range NOE connectivities, identification of slowly exchanging amide protons, and $^3J_{NH\alpha}$ coupling constants. The lower case letters identify an N-terminal dipeptide segment that originates from the overexpression system. Boxes above the sequence represent amide protons with exchange rate constants $< 7 \cdot 10^{-2}$ min^{-1} in D_2O solution at pD = 6.0 and 22°C. Below the sequence the NOE connectivities are indicated where the thickness of the bars for the sequential connectivities represents the NOE intensities. The magnitude of the vicinal scalar coupling constants $^3J_{NH\alpha}$ is represented by a black bar below the NOE connectivities, which covers the range from 10 ± 1 Hz (Thr^{74}) to 3 ± 1 Hz (Asp^{70}). The sequence locations of the secondary structure elements identified from the data in this figure and the structure calculations with the program DIANA are indicated at the bottom.

straints based on local NOE distance constraints and on the scalar coupling constants $^3J_{NH\alpha}$ were generated with the program HABAS [47]. Structure calculations were done using the program DIANA [46,48] with four REDAC cycles, where the maximal target function value per residue for locally acceptable segments was set to $C^{(1)}$ = 0.6 Å^2, $C^{(2)}$ = 0.4 Å^2, $C^{(3)}$ = 0.4 Å^2 and $C^{(4)}$ = 0.3 Å^2, respectively [49].

3. RESULTS

Fig. 1 shows the 125-residue hSCP2 polypeptide obtained from the overexpression system used, where the first two residues are not part of natural hSCP2. For a general characterization, the thermal denaturation was monitored by Circular Dichroism (CD) at 222 nm, which yielded a melting point of about 70°C at pH = 6.0, whereby the unfolding was irreversible. The maximal solubility of hSCP2 in H_2O at pH = 6.0 containing 15 mM phosphate buffer was found to be approximately 1.5 mM at 22°C. Due to the single Cys^{71} (Fig. 1), hSCP2 is prone to oxidative dimerization at higher concentrations, and therefore all measurements were performed in the presence of 5 mM DTT under

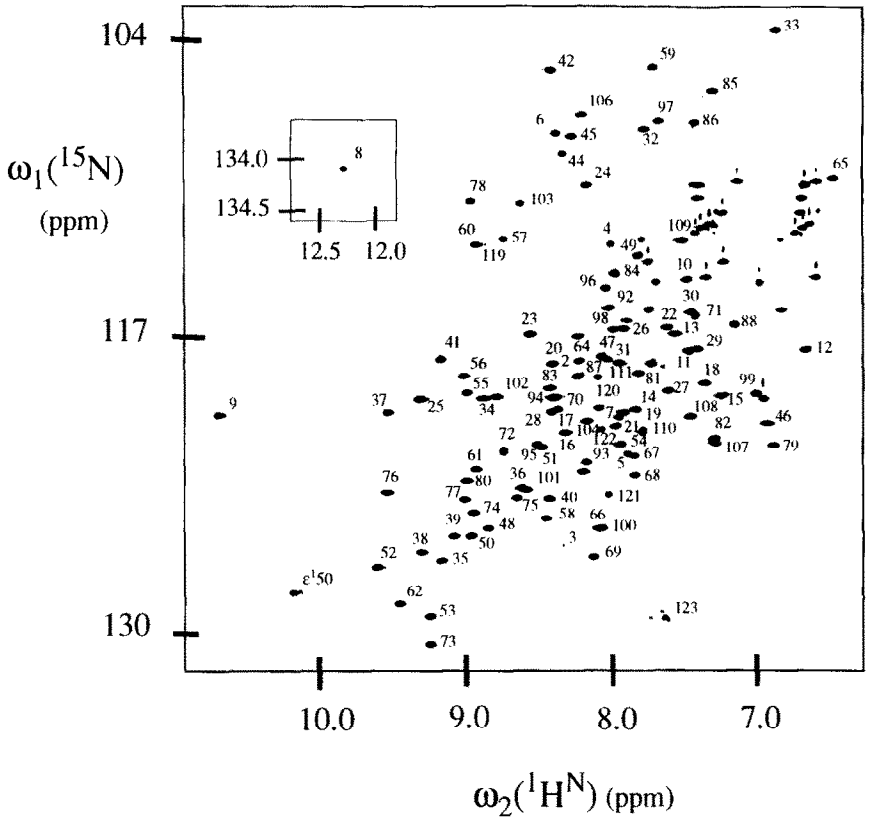

Fig. 2. Contour plot of a 2D [^{15}N,^{1}H]-HSQC spectrum of hSCP2 uniformly labeled with ^{15}N, (^{1}H frequency = 600 MHz, protein concentration = 1.3 mM in 90% H_2O/10% D_2O with 15 mM KH_2PO_4/5 mM DTT, pH = 6.0, T = 36°C). The cross peaks are marked with the amino acid residue numbers.

Argon. A 2D [^{15}N,^{1}H]-HSQC spectrum recorded at 36°C (Fig. 2) shows good chemical shift dispersion in both dimensions, but the signals of some residues are very weak, which is probably due to conformational exchange processes on a millisecond time scale. We subsequently recorded NMR spectra at multiple temperatures in order to obtain complementary information for those residues that are affected by these presumed exchange processes.

3.1. *Sequence-specific resonance assignments*

The 2D [^{15}N,^{1}H]-HSQC spectrum of Fig. 2 was the starting point for obtaining sequence-specific ^{1}H resonance assignments of hSCP2. Using the program XEASY (C. Bartels, T.H. Xia, M. Billeter, P. Güntert and K. Wüthrich, to be published), the ^{15}N and ^{1}H chemical shifts obtained from Fig. 2 were taken to define the corresponding positions along $\omega_2(^{15}N)$ and $\omega_3(^1H)$ in a 3D ^{15}N-resolved [^{1}H,^{1}H]-TOCSY experiment [37,38]. Comparison with the 3D *ct*-HNNHB spectrum [40,41] enabled the unambiguous identification of the β-proton resonances of 49 out of the 105 non-prolyl and non-glycyl spin systems. For 21 additional spin systems one of the two β-resonances could be assigned. 9 out of the 10 alanines could be identified and were used together with the 15 glycines as starting points for the sequential resonance assignment. Using the peak positions of the 3D ^{15}N-resolved [^{1}H,^{1}H]-TOCSY and the 3D *ct*-HNNHB spectrum, the intraresidual NOE connectivities in a 3D ^{15}N-resolved [^{1}H,^{1}H]-NOESY experiment [37–39] were distinguished from the sequential $d_{\alpha N}$, d_{NN} and $d_{\beta N}$ NOE connectivities [50,51]. As an illustration, Fig. 3 shows the data used for the assignments from residues 13–22 as a composite plot of strips taken from the 3D ^{15}N-resolved [^{1}H,^{1}H]-NOESY spectrum recorded at 36°C. The same procedure was repeated at 28°C, and some NOE connectivities identified only at this temperature are also included in Fig. 1. The chemical shift at 28°C and 36°C were found to be nearly identical.

Overall, sequence-specific polypeptide backbone assignments were obtained for the 109 residues 2–42, 44–62, 64–88, 92–104, 106–111 and 119–123; at least one sequential connectivity was found for all pairs of assigned neighbouring residues (Fig. 1). For 69 residues the complete ^{1}H spin systems could be assigned, and for an additional 38 residues it was possible to identify the β-proton resonances in addition to the backbone resonances. The resulting ^{1}H and the ^{15}N chemical shifts will be presented elsewhere.

3.2. *Assignment of the aromatic spin systems*

The aromatic spin systems were assigned using the standard strategy for unlabeled proteins [51]. For the

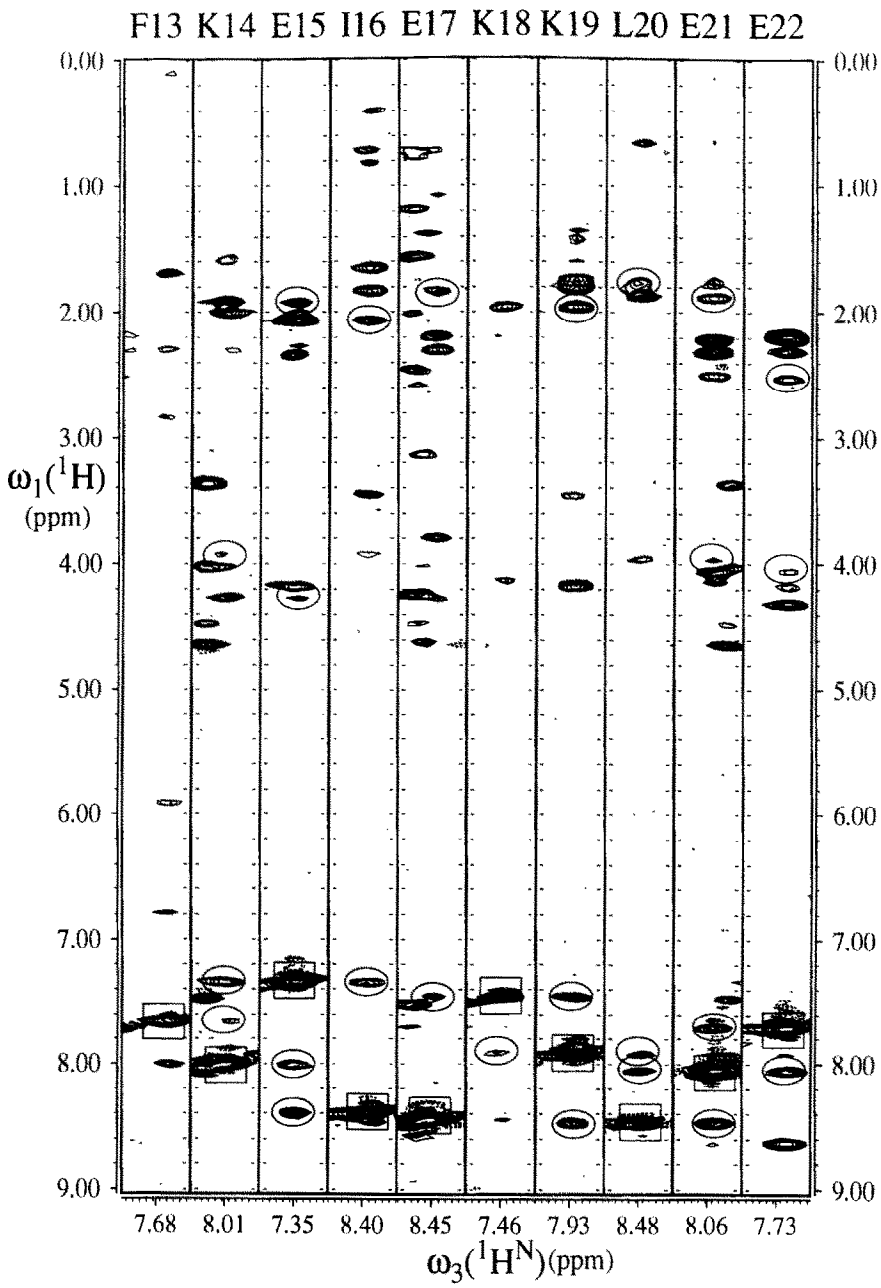

Fig. 3. Composite plot of $\omega_1(^1H)$–$\omega_3(^1H)$ strips taken from the 3D ^{15}N-resolved [^1H,^1H]-NOESY spectrum of hSCP2 at 36°C, which shows the sequential connectivities in the α-helical polypeptide segment from Phe[13] to Glu[22] (protein concentration 1.3 mM, solvent 90% H_2O/10% D_2O with 15 mM KH_2PO_4 and 5 mM DTT, pH = 6.0, mixing time = 100 ms, ^1H frequency 600 MHz). The individual strips with a width of 0.1 ppm along ω_3 were taken from $\omega_1(^1H)$–$\omega_3(^1H)$ planes at different $\omega_2(^{15}N)$ chemical shifts and centred about the amide proton chemical shift of the residue indicated at the top. The strips are ordered according to the amino acid sequence. Squares and circles identify the diagonal peaks of the amide protons, and the sequential d_{NN}, $d_{\alpha N}$ and $d_{\beta N}$ connectivities, respectively (see also Fig. 1).

unique spin system of Trp[50], the ε^1- and δ^1-proton resonances were identified in the 3D ^{15}N-resolved spectra, and the other ring protons were assigned in a 2D ^1H-NOESY spectrum recorded in D_2O and a $^{15}N(\omega_1,\omega_2)$-double-half-filtered [$^1H$,$^1H$]-NOESY spectrum recorded in H_2O. The eight Phe rings exhibit sufficiently large chemical shift dispersion so that NOE connectivities of the δ-protons with the α- and/or β-protons could thus be unambiguously identified, and the resonances of the ε- and ζ-ring protons were subsequently identified by combined use of 2D NOESY and 2D TOCSY spectra. In addition, for seven of the eight phenylalanines, NOEs from the δ-protons to the backbone amide protons were observed in 3D ^{15}N-resolved [^1H,^1H]-NOESY spectra.

3.3. *Secondary structure of hSCP2*

A large number of medium-range and long-range NOEs could be identified in the 3D ^{15}N-resolved

[^{1}H,^{1}H]-NOESY spectra recorded at 28°C and 36°C. The sequential and medium-range connectivities together with the $^3J_{NH\alpha}$ coupling constants and the identification of slowly exchanging amide protons (Fig. 1) resulted in the determination of three helices and five β-strands. Four criteria were used to support the presence of the helices: (i) $^3J_{NH\alpha}$ coupling constants < 6.0 Hz [52]; (ii) strong sequential d_{NN} connectivities [50]; (iii) a significant number of $d_{\alpha N(i,i+3)}$ connectivities characteristic of α-helices [53]; (iv) slow amide proton exchange rates for most residues in the helical polypeptide segments [51]. The helices A, B and C were thus found in the polypeptide segments 9–22, 25–30 and 78–84 (Figs. 1 and 4A). Due to the long preparation time of about 5 h for the D_2O sample, only an incomplete set of slowly exchanging amide protons was registered.

The identification of the β-strands and their relative orientation in the β-sheet was based upon: (i) $^3J_{NH\alpha}$ coupling constants > 8.0 Hz [52]; (ii) strong sequential $d_{\alpha N}$ connectivities [50]; (iii) a significant number of interstrand $d_{\alpha N}$ and d_{NN} connectivities defining the topology of the β-sheet [51]; (iv) alternating slow and fast amide

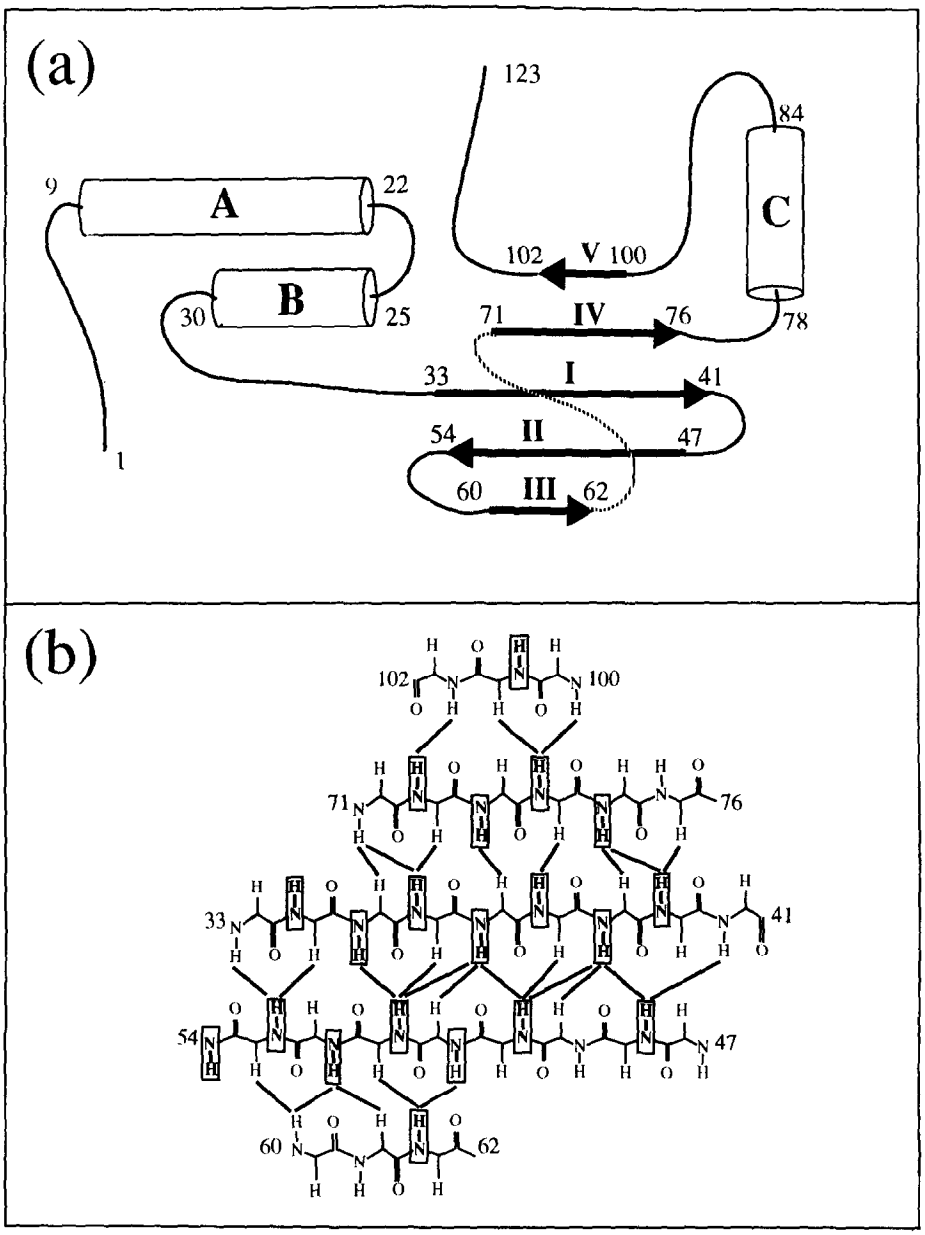

Fig. 4. (A) Secondary structure elements and topology of the β-sheet of hSCP2 identified on the basis of sequential and medium-range NOEs (see also Fig. 1) and long-range backbone–backbone interstrand NOEs in the β-sheet. The start and the end of the secondary structure elements, as well as the N- and the C-terminus of the polypeptide chain are marked with their sequence locations. The dashed line connecting residues 62 and 71 indicates that the polypeptide chain crosses below the plane defined by the β-sheet. (B) The five-stranded β-sheet of hSCP2 in the same orientation as in (A). Thin lines identify assigned interstrand NOEs and slowly exchanging amide protons are marked with boxes (see also Fig. 1).

proton exchange rates in the peripheral strands of the β-sheet, and continuous stretches of residues with slowly exchanging amide protons in the central strands [51]. Using the criteria (i) and (ii) we identified five β-strands with residues 33–41, 47–54, 60–62, 71–76 and 100–102. The amide proton exchange data (Fig. 1) suggested that strands 3 and 5 are peripheral, whereas continuous stretches of slowly exchanging amide protons supported that strands 1, 2 and 4 are in non-peripheral locations. 28 interstrand backbone-backbone NOE connectivities revealed the presence of a mixed, five-stranded β-sheet. The first three strands comprising residues 33–41, 47–54 and 60–62, are arranged in an antiparallel fashion, the polypeptide chain then crosses over this three-stranded sheet in a right-handed sense so that the fourth strand with residues 71–76 is added parallel to the first one. The fifth strand comprising residues 100–102 runs antiparallel to the fourth one, so that the overall topology [54] is +1, +1, −3x, −1 (Fig. 4).

3.4. *Calculation of the three-dimensional polypeptide fold*

For a preliminary calculation of the complete three-dimensional structure of hSCP2 we used an input of 625 NOE upper distance constraints (235 intraresidual, 123 sequential, 87 medium-range and long-range backbone–backbone, and 180 interresidual constraints with side chain protons) derived from the homonuclear 2D ^{1}H-NOESY spectra and the 3D ^{15}N-resolved [^{1}H,^{1}H]-NOESY spectra recorded at 28°C and 36°C. In addition, the input contained 95 vicinal $^{3}J_{NH\alpha}$ scalar coupling constants. Thus, although no amino acid side chain conformations are discussed in this paper, the calculation of the backbone fold was based on assignments of numerous medium-range and long-range NOE distance constraints that also include side chain hydrogen atoms. The following local average pairwise RMSD values relative to the mean structures were obtained for the residues forming the secondary structure elements: 0.88 Å for helix A (residues 9–22), 0.69 Å for helix B (25–30), 1.24 Å for helix C (78–84) and 1.28 Å for the β-sheet (33–41, 47–54, 60–62, 71–76, 100–102), showing that all regular secondary structure elements that have been identified are locally well defined. Fig. 5 shows a superposition of the backbone heavy atoms of helices A and B and the β-sheet of the 20 DIANA conformers with the lowest target function value. The average pairwise root mean squared deviation (RMSD) after superposition of the backbone atoms N, C^{α} and C′ relative to their mean structure was calculated to be 2.0 Å for this substructure of hSCP2 comprising the residues 9–22, 25–30, 35–40, 47–54, 71–76 and 100–102. The relative orientation of the helices A and B and the β-sheet is quite well defined, but the orientation of helix C relative to the remainder of the molecule is not yet well defined. Fig. 5B shows a ribbon drawing of the residues 8–76 and 99–103 of the DIANA conformer of hSCP2 with the lowest target function, which includes all regular secondary structure elements except for helix C.

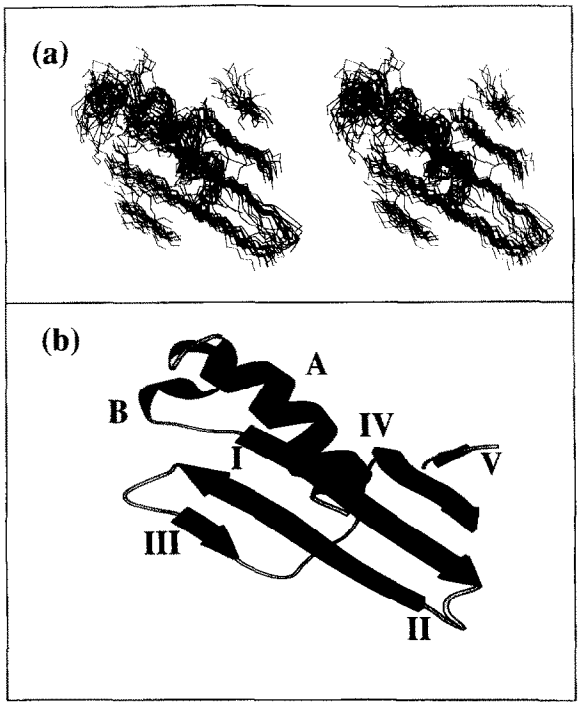

Fig. 5. Three-dimensional arrangement of the β-sheet and the helices A and B as obtained from DIANA structure calculations. (A) Stereo view of the polypeptide backbone heavy atom representation of the 20 DIANA conformers of hSCP2 with the lowest target function values, which were superimposed for minimal RMSD of the backbone atoms N, C^{α} and C′ of the residues in the helices A and B and the β-sheet. (B) Ribbon drawing generated with the program MOLSCRIPT [56] of residues 8–76 and 99–103 of the DIANA conformer of hSCP2 with the lowest target function value, comprising all regular secondary structure elements except helix C. The helices and β-strands are labeled as in Fig. 1.

4. DISCUSSION

A preliminary evaluation of previously reported effects of site-directed mutagenesis on SCP2 activity [22] in the light of the presently described regulary secondary structure and the three-dimensional polypeptide backbone fold of hSCP2 leads to the following intriguing observations. (i) Whereas N-terminal deletion of 7 amino acid residues had only a relatively small effect, deletion of 12 residues, which directly affects the helix A from residues 9 to 22, resulted in almost complete loss of activity. In a different experiment, disruption of the amphipathicity of helix A resulted in complete loss of activity [22], providing additional indication that this helix represents an essential structural element for the lipid transport activity of SCP2. However, whether helix A participates in the formation of a hydrophobic lipid binding site or is involved in stabilizing the overall fold of the protein cannot presently be answered. We hope that ongoing studies of the interaction of SCP2

with different transport substrates will answer this question. (ii) The region from Met^{105} to the C-terminus was shown to be of minor importance for the lipid transport activity, as C-terminal deletion of 18 residues resulted in high residual activity, whereas deletion of 5 additional residues to Lys^{100} resulted in almost complete inactivation [22]. Therefore, it was concluded from the functional evidence that residues between positions 100 and 104 are essential for SCP2 activity. Interestingly, we now find that residues 100 to 102 form the small β-strand V (Fig. 4), which participates in the formation of the central β-sheet. (iii) Substitution of Asn^{104}, which is located in close vicinity of the β-strand V, with different amino acids also has profound effects on SCP2 activity. Taken together, these findings indicate that residues within or close to the core part of the protein with the helices A, B and C and the β-strands I to V appear to be sufficient for the lipid transport activity of SCP2.

The NMR determination of the regular secondary structure elements and the preliminary structure calculations revealed a distinctive α–β tertiary fold (Fig. 5B) for hSCP2. No near-identity can be found with any of the protein folding types that have recently been surveyed by Thornton's group [55]. Furthermore, a sequence homology search using the SWISS-PROT data bank did not yield any sequence with a homology larger than 30% identity, with the sole exception of PXP18, which is a yeast homologue of hSCP2. It therefore seems quite likely that elucidation of the mechanisms by which hSCP2 mediates lipid transfer might lead to the discovery of a novel mechanism of protein-mediated sterol and lipid transfer.

Acknowledgements: Financial support was obtained from the Schweizerischer Nationalfonds (Project 31.32033.91), Deutsche Forschungsgemeinschaft (Grant Se 459/2-1), Bristol-Myers Squibb and the Swedish Medical Research Council (Fellowship to J.J.). The use of the Cray Y-MP of the ETH Zürich and the NEC SX3 supercomputer of the Centro Svizzero di Calcolo Scientifico is gratefully acknowledged. We thank R. Marani for the careful processing of the manuscript.

REFERENCES

[1] Reinhart, M.P. (1990) Experientia 46, 599–611.
[2] Wirtz, K.W.A. (1991) Annu. Rev. Biochem. 60, 73–99.
[3] Van Amerongen, A., Demel, J., Westerman, J. and Wirtz, K.W.A. (1989) Biochim. Biophys. Acta 1004, 36–43.
[4] Wirtz, K.W.A. and Gadella Jr., T.W.J. (1990) Experientia 46, 592–599.
[5] Noland, B.J., Arebalo, R.E., Hansbury, E. and Scallen, T.J. (1980) J. Biol. Chem. 255, 4282–4289.
[6] Gavey, K.L., Noland, B.J. and Scallen, T.J. (1981) J. Biol. Chem. 256, 2993–2999.
[7] Poorthuis, B.J.H.M. and Wirtz, K.W.A. (1982) Biochim. Biophys. Acta 710, 99–105.
[8] Traszkos, J.M. and Gaylor, J.L. (1983) Biochim. Biophys. Acta 751, 52–65.
[9] Seltman, H., Diven, W., Rizk, M., Noland, B.J., Chanderbhan, R., Scallen, T.J., Vahouny, G.V. and Sanghvi, A. (1985) Biochem. J. 230, 19–24.
[10] Lidström-Olsson, B. and Wikvall, K. (1986) Biochem. J. 238, 879–884.
[11] Chanderbhan, R., Noland, B.J., Scallen, T.J. and Vahouny, G. (1982) J. Biol. Chem. 257, 8928–8934.
[12] Vahouny, G.V., Dennis, P., Chanderbhan, R., Fisku, G., Noland, B.J. and Scallen, T.J. (1984) Biochem. Biophys. Res. Commun. 122, 509–515.
[13] Vahouny, G.V., Chanderbhan, R., Noland, B.J., Irwin, D., Dennis, P., Lambeth, J.D. and Scallen, T.J. (1983) J. Biol. Chem. 258, 11731–11737.
[14] Tan, H., Okazaki, K., Kubota, I., Kamiryo, T. and Utiyama, H. (1990) Eur. J. Biochem. 190, 107–112.
[15] Ossendorp, B.C., van Heusden, G.P.H. and Wirtz, K.W.A. (1990) Biophys. Res. Commun. 168, 631–636.
[16] Billheimer, L.T., Strehl, L.L., Davis, G.L., Strauss III, J.F. and Davis, L.G. (1990) DNA Cell Biol. 9, 154–163.
[17] Seedorf, U. and Assmann, G. (1991) J. Biol. Chem. 266, 630–636.
[18] Mori, T., Tsukamoto, T., Mori, H., Tashiro, Y. and Fujiki, Y. (1991) Proc. Natl. Acad. Sci. USA 88, 4338–4342.
[19] Moncecchi, D., Pastuszyn, A. and Scallen, T.J. (1991) J. Biol. Chem. 266, 9885–9892.
[20] Yamamoto, R., Kallen, C.B., Babalola, G.O., Rennert, H., Billheimer, J.T. and Strauss III, J.F. (1991) Proc. Natl. Acad. Sci. USA 88, 463–467.
[21] Crain, R.C. and Zilversmit, D.B. (1980) Biochemistry 19, 1433–1439.
[22] Seedorf, U., Scheek, S., Engel, T., Steiff, M., Hinz, H.J. and Assmann, G. (1993) J. Biol. Chem. (in press).
[23] Gadella, T.W.J., Bastiaens, P.I.H., Visser, A.J.W.G. and Wirtz, K.W.A. (1991) Biochemistry 30, 5555–5564.
[24] Smith, D.B. and Johnson, K.S. (1988) Gene 67, 31–40.
[25] Johnson, K.S., Harrison, G.B.L., Lightowlers, M.W., O'Hoy, K.L., Cougle, W.G., Dempster, R.P., Lawrence, S.B., Vinton, J.G., Heath, D.D. and Rickard, M.D. (1989) Nature 338, 585–587.
[26] Bradford, M.M. (1976) Anal. Biochem. 72, 248–254.
[27] Marion, D., Ikura, K., Tschudin, R. and Bax, A. (1989) J. Magn. Reson. 85, 393–399.
[28] Güntert, P., Dötsch, V., Wider, G. and Wüthrich, K. (1992) J. Biomol. NMR 2, 619–629.
[29] Anil-Kumar, Ernst, R.R. and Wüthrich, K. (1980) Biochem. Biophys. Res. Commun. 95, 1–6.
[30] Griesinger, C., Otting, G., Wüthrich, K. and Ernst, R.R. (1988) J. Am. Chem. Soc. 110, 7870–7872.
[31] Marion, D., Ikura, K. and Bax, A. (1989) J. Magn. Reson. 84, 425–430.
[32] DeMarco, A. and Wüthrich, K. (1976) J. Magn. Reson. 24, 201–204.
[33] Güntert, P. and Wüthrich, K. (1992) J. Magn. Reson. 96, 403–407.
[34] Otting, G. and Wüthrich, K. (1988) J. Magn. Reson. 76, 569–574.
[35] Shaka, A.J., Keeler, J., Frenkiel, T. and Freeman, R. (1983) J. Magn. Reson. 52, 113–118.
[36] Bodenhausen, G. and Ruben, D. (1980) Chem. Phys. Lett. 69, 185–188.
[37] Fesik, S.W. and Zuiderweg, E.R.P. (1988) J. Magn. Reson. 78, 588–593.
[38] Marion, D., Kay, L.E., Sparks, S.W., Torchia, D.A. and Bax, A. (1989) J. Am. Chem. Soc. 111, 1515–1517.
[39] Messerle, B.A., Wider, G., Otting, G., Weber, C. and Wüthrich, K. (1989) J. Magn. Reson. 85, 608–613.
[40] Chary, K.V.R., Otting, G. and Wüthrich, K. (1991) J. Magn. Reson. 93, 218–224.
[41] Archer, S.J., Ikura, U., Torchia, D.A. and Bax, A. (1991) J. Magn. Reson. 95, 636–641.
[42] Stephenson, D.S. (1988) Prog. NMR Spectrosc. 20, 516–626.
[43] Otting, G. and Wüthrich, K. (1990) Q. Rev. Biophys. 23, 39–96.
[44] Szyperski, T., Güntert, P., Otting, G. and Wüthrich, K. (1992) J. Magn. Reson. 99, 552–560.

[45] Eccles, C., Güntert, P., Billeter, M. and Wüthrich, K. (1991) J. Biomol. NMR 1, 111–130.
[46] Güntert, P., Braun, W. and Wüthrich, K. (1991) J. Mol. Biol. 217, 517–530.
[47] Güntert, P., Braun, W., Billeter, M. and Wüthrich, K. (1989) J. Am. Chem. Soc. 111, 3997–4004.
[48] Güntert, P., Qian, Y.Q., Otting, G., Müller, M., Gehring, W.J. and Wüthrich, K. (1991) J. Mol. Biol. 217, 531–540.
[49] Güntert, P. and Wüthrich, K. (1991) J. Biomol. NMR 1, 447–456.
[50] Billeter, M., Braun, W. and Wüthrich, K. (1982) J. Mol. Biol. 155, 321–346.
[51] Wüthrich, K. (1986) NMR of Proteins and Nucleic Acids, Wiley, New York.
[52] Pardi, A., Billeter, M. and Wüthrich, K. (1984) J. Mol. Biol. 180, 741–751.
[53] Wüthrich, K., Billeter, M. and Braun, W. (1984) J. Mol. Biol. 180, 715–740.
[54] Richardson, J. (1981) Adv. Protein Chem. 34, 167–339.
[55] Orengo, C.A., Flores, T.P., Taylor, W.R. and Thornton, J.M. (1993) Protein Eng. 6, 485–500.
[56] Kraulis, P.J. (1991) J. Appl. Crystallogr. 24, 946–950.